Journal of Fluorescence, Vol. 14, No. 3, May 2004 (©2004)

Photobleaching, Mobility, and Compartmentalisation: Inferences in Fluorescence Correlation Spectroscopy

A. Delon,[1,4] Y. Usson,[2] J. Derouard,[1] T. Biben,[1] and C. Souchier[3]

Received October 18, 2003; accepted December 8, 2003

In living cells the transport and diffusion of molecules is constrained by compartments of various sizes. This paper is an attempt to show that the size of these compartments can in principle be estimated experimentally from Fluorescence Correlation Spectroscopy (FCS) combined with the measurement of the photobleaching rate. In this work, confocal fluorescence microscopy experiments have been carried out on giant unilamellar vesicles, a system that mimics cellular compartmentalisation. We have developed numerical and analytical models to describe the fluorescence decay due to photobleaching in this geometry, which has enabled us to point out two regimes depending on the value of the parameter $p_B = \sigma_B P/D$ (where σ_B is the photobleaching cross section of the dye, D its diffusion constant, and P the laser power (in photon/s)). In particular, when $p_B \ll 1$ (i.e. in the fast diffusion regime), the photobleaching rate is independent of the diffusion constant and scales like $\sigma_B P/R^2$, in agreement with the experimental results. On the other hand, the standard diffusion models used to analyse the FCS data do not take into account the effects of the fluorescence decay on the autocorrelation curve. We show here how to correct the raw data for these drawbacks.

KEY WORDS: Photobleaching; fluorescence correlation spectroscopy; compartmentalisation; molecular diffusion; confocal microscopy.

INTRODUCTION

Fluorescence Correlation Spectroscopy (FCS) is an analytical method used to measure molecular concentrations and diffusion coefficients by monitoring the fluctuations of the fluorescence signal arising from a microvolume during the sampling time (typically between 10 and 30 s) [1–5]. In FCS, the confocal laser microscopy set up restricts the size of the microvolume down to 1 fl and the detection device (Avalanche photodiode) enables the analysis of sub-nanomolar concentrations, thus making FCS well suited for sparse molecule detection. Diffusion coefficients are a function of the molecular weight, the conformation, the medium viscosity and the microenvironment. FCS makes it possible quantitative study of molecular interactions in solution and in living cells.

A major difficulty that one has to face with when performing FCS, under 1 photon excitation, is the irreversible photobleaching of fluorochromes [6–10]. This phenomenon manifests as a monotonous decrease of the fluorescence count rate. From the point of view of FCS, three distinct effects can be observed in the correlation curve $G(\tau)$: i) an increase of the amplitude $G(0)$, that corresponds to the decreasing concentration of intact fluorochromes; ii) a shortening of the apparent diffusion time at high laser intensities, that corresponds to the photodestruction of fluorescent molecules within the confocal volume; iii) a strong alteration of the shape of the autocorrelation curve $G(\tau)$, if the fluorescence count rate decay time is not large compared with the sampling time. Surprisingly, the third item has been reported for the first time in the literature, only very recently [11,12]. This is

[1] LSP, CNRS UMR5588, Université Joseph Fourier, BP 87, 38402 Saint Martin d'Hères Cedex, France.
[2] TIMC, CNRS UMR5525, Université Joseph Fourier, IAB, Domaine de la Merci, 38706 La Tronche Cedex, France.
[3] INSERM U309, Université Joseph Fourier, IAB, Domaine de la Merci, 38706 La Tronche Cedex, France.
[4] To whom correspondence should be addressed. E-mail: adelon@ujf-grenoble.fr

1053-0509/04/0500-0255/0

probably due to the fact that the usual strategy, especially when studying protein dynamics in living cells, consists in avoiding strong photobleaching effects by using more stable fluorophores and optimising the fluorescence count rate per molecule. Consequently, numerous efforts have been aimed at understanding the molecular dynamics and kinetics of photo-destruction, notably in the framework of single molecule detection [13–18].

In this paper we show that it is possible to take advantage of the photocount decay rate to get information about the compartmentalisation. As a matter of fact, the fluorescence decay rate observed at long times can be related to the size of the compartment, in contrast to the photobleaching behaviour observed at times shorter than the mean dwell time within the confocal volume. These general features of photobleaching were pointed out for the first time by Peters *et al.* in the eighties and leaded to the so called Continuous Fluorescence Microphotolysis technique, applied for lateral 2D diffusion in membranes [19] and later on in 3D [20]. Recently, Langowski [21], showed that diffusion and binding of molecules to specific sites could be measured by combining Continuous Fluorescence Photobleaching (i.e. Continuous Fluorescence Microphotolysis), FCS and Confocal Laser Scanning Microscopy (CLSM). Continuous Fluorescence Photobleaching/Microphotolysis is tightly linked with Fluorescence Recovery After Photobleaching (FRAP) [22] and Fluorescence Loss In Photobleaching (FLIP) [23]. In both techniques the fluorophores of a particular region are made non-fluorescent by applying very high intensity illumination. In FRAP the subsequent kinetics of the fluorescence recovery in the very same bleached volume is recorded, while in FLIP the loss of fluorescence from outside the bleached region is monitored. FLIP provides compartmental information about boundaries within the cell and, from that point of view, presents similarities with Continuous Fluorescence Microphotolysis. However the above mentioned techniques are not single molecule techniques and thus do not permit to get the concentration of the various components to which a fluorophore is attached. Conversely, by performing continuous fluorescence photobleaching with nanomolar concentrations of fluorophores, it must be possible to get information about both compartmentalisation and diffusion.

The goal of the present study is then to rationalise the relation between mobility (diffusion), photobleaching and compartmentalisation, in the experimental conditions encountered when performing FCS. Experiments have been performed on giant unilamellar vesicles, as a model for cell compartmentalisation.

In the Materials and Methods section we present experimental and numerical techniques; in the Experimental Results section the theoretical, numerical and experimental data are presented and briefly discussed while the general discussion and conclusion are given in the Discussion and Conclusion section.

MATERIALS AND METHODS

Preparation of Giant Unilamellar Vesicles

Giant phospholipidic vesicles were swollen from L-a dioleyol-phosphatidylcholine using the electroformation method [24]. They were prepared in sucrose solutions (typically 40 mM) containing the fluorochromes with a concentration of 20 nM: Lucifer Yellow-CH (LY-CH) from Molecular Probes or Fluorescein-5- isothiocyanate (FITC) from Sigma. They were then diluted in glucose solutions of equal osmolalities, where they could sedimentate. For reasons of consistency, the experiments performed in solution were done with the inner solution of the vesicles.

Dye Penetration in Living Cells

HeLa cells were cultured on Lab-tek chambered coverglass (Nunc). FITC was loaded into cells using influx Pincoytic Cell-loading reagent (Molecular Probes, USA). Cells were measured in HBSS (Ca^{++} Mg^{++}) medium buffered with Hepes at 37°C.

Data Acquisition

FCS measurements were performed on a FCS-CLSM confocal microscope system (Confocor 2, Zeiss, Germany) using a 40 × water immersion objective lens (C-Apochromat, 1.2 NA) and high sensitivity avalanche photodiodes (APD). The values of the laser power used for the experiment were measured with a calibrated photodiode immersed in a drop of water covering the front pupil of the objective lens. A correspondence table is given (Table I), that relates the measured laser powers of the 488-nm line (used for FITC) and of the 457-nm line (used for LY-CH) to the laser attenuation scale of the Confocor 2 software. Note that this correspondence table may be valid for our system only, since it is sensitive to the age of the laser tube, the adjustments of the Acousto Optic Tunable Filter (AOTF) used to attenuate the laser power, etc.

Data Processing

The intensity decays observed in vesicles were fitted with multi-exponential laws:

$$I(t) = A_0 + A_1\, e^{-t/\tau_1} + A_2\, e^{-t/\tau_2} \qquad (1)$$

Table I. Output Optical Powers of the Confocor 2 System, Versus the Attenuation Scale of the 488 and 457 Laser Lines

Confocor scale (%)	Output power 488 nm (mW)	Output power 457 nm (mW)
0.1	4.4×10^{-3}	1.1×10^{-2}
0.2	4.8×10^{-3}	1.2×10^{-2}
0.5	6.5×10^{-3}	1.3×10^{-2}
1	9.5×10^{-3}	1.6×10^{-2}
2	1.3×10^{-2}	1.9×10^{-2}
5	4.2×10^{-2}	4.3×10^{-2}
10	8.5×10^{-2}	8.3×10^{-2}
20	1.7×10^{-1}	1.6×10^{-1}
50	4.2×10^{-1}	4.0×10^{-1}
100	9.6×10^{-1}	8.1×10^{-1}

Note. At 488 nm the laser power is set to 25%, while it is set to 100% for the 457 line.

It is worth to note that, while two exponential decays were necessary for LY-CH, FITC data could be fitted by fixing A_2 to 0.

The autocorrelation curves were calculated, from the raw data set, using a home made program developed in a C^{++} environment (Microsoft Visual C^{++}):

$$G_D(\tau) = \frac{\langle I(t)I(t+\tau)\rangle}{\langle I(t)\rangle^2} = 1 + \frac{\langle \delta I(t)\delta I(t+\tau)\rangle}{\langle I(t)\rangle^2} = 1 + g_D(\tau) \qquad (2a)$$

with $I(t) = \langle I(t)\rangle + \delta I(t)$. From a theoretical point of view $\langle I(t)\rangle$ is an ensemble average, but in practice it is obtained by averaging over the time of acquisition. When photobleaching was not observed, the autocorrelation curves were fitted with the standard formula used for translational diffusion, in presence of a triplet dynamics, that is:

$$g_D(\tau) = \frac{1}{N}\left(1 + \frac{T_{eq}}{1 - T_{eq}} e^{-\frac{\tau}{\tau_T}}\right) \frac{1}{\left(1 + \frac{\tau}{\tau_D}\right)\left(1 + \frac{\tau}{S^2\tau_D}\right)^{1/2}} \qquad (2b)$$

where N is the number of molecules in the confocal volume, T_{eq} is the fraction of molecules in the triplet state, τ_T is the characteristic triplet time, τ_D is the diffusion time and S is the structure parameter [3–5].

When the fluorescence count rate is still stationary, it is possible to take into account the photobleaching by using the model proposed by Enderlein [25] or by Widengren [8]. The formula suggested by the latter author is used most of the time:

$$G_B(\tau) = 1 + e^{-k_B t} \times g_D(\tau) \qquad (3)$$

where k_B is the photobleaching rate within the confocal volume.

However, when the fluorescence decay rate is large, it is necessary to correct the raw data set before calculating the autocorrelation curves. Two different methods have been used.

i) The first method consists in dividing the photocount stream into short and equal time slices (typically 1 s long), during which the count rate decrease is weak, such that the corresponding autocorrelation functions are not biased by the photobleaching. Then, the S/N ratio can be improved by averaging this series of autocorrelation functions.

ii) The second one consists in rectifying the raw data by replacing the numbers, N_i, of photocounts detected at times $t_1, t_2, \ldots$ by the corrected amplitudes A_i:

$$A_i = \frac{I_0}{\langle I\rangle_i} N_i \qquad (4)$$

where I_0 can be chosen to be the initial intensity and $\langle I\rangle_i$ is the locally averaged count rate at time t_i. $\langle I\rangle_i$ can be evaluated by various means such as multi-exponential fit, cubic spline, adjacent averaging, etc. (note that, due to the high sampling rate necessary to perform FCS, N_i is most of the time nil). Thanks to this correction, the locally averaged corrected count rate,

$$\frac{\sum_{i=1}^{n} A_i}{t_n - t_1},$$

becomes constant.

Although the corrected raw data are then autocorrelated as usual, one must pay some attention to the amplitude of the autocorrelation function calculated with the corrected intensity $I'(t)$. Let's consider, $G'(\tau)$, the ensemble averaged autocorrelation function evaluated at time t:

$$G'(\tau) = \frac{\langle I'(t)I'(t+\tau)\rangle}{\langle I'(t)\rangle^2} \qquad (5a)$$

where, according to Eq. (4), $I'(t) = \frac{I_0}{\langle I\rangle_t} I(t)$, $\langle I\rangle_t$ being a local average of $I(t)$ around time t. In fact, since the autocorrelation function in based on ensemble averages, one must rather write $I'(t) = \frac{I_0}{\langle I(t)\rangle} I(t)$, where $\langle I(t)\rangle$ is the ensemble averaged intensity at time t. Then, by writing $I(t) = \langle I(t)\rangle + \delta I(t)$ and thus $I'(t) = I_0[1 + \frac{\delta I(t)}{\langle I(t)\rangle}]$, Eq. (5a) can be rewritten:

$$G'(\tau) = \left\langle \left[1 + \frac{\delta I(t)}{\langle I(t)\rangle}\right]\left[1 + \frac{\delta I(t+\tau)}{\langle I(t+\tau)\rangle}\right]\right\rangle = 1 + \left\langle \frac{\delta I(t)}{\langle I(t)\rangle}\frac{\delta I(t+\tau)}{\langle I(t+\tau)\rangle}\right\rangle \qquad (5b)$$

Since the intensity, I, is proportional to the number of fluorescent molecules in the confocal volume, N, one is

left with the quantity $\langle \frac{\delta N(t)}{\langle N(t)\rangle} \frac{\delta N(t+\tau)}{\langle N(t+\tau)\rangle} \rangle$. There are two contributions to the molecule number variations: the fast thermodynamical fluctuations and the slow decrease due to photobleaching. This can be taken into account by writing $\delta N(t) = \sqrt{\langle N(t)\rangle}\,\varepsilon(t)$, where $\varepsilon(t)$ represents the thermodynamical fluctuations corresponding to $\langle N(t)\rangle = 1$ (that is, $\langle \varepsilon(t)^2\rangle = 1$). Equation (5b) thus becomes:

$$G'(\tau) = 1 + \frac{h(\tau)}{[\langle N(t)\rangle\langle N(t+\tau)\rangle]^{1/2}} \tag{5c}$$

where $h(\tau) = \langle \varepsilon(t)\,\varepsilon(t+\tau)\rangle$ is the autocorrelation function corresponding to $\langle N(t)\rangle = 1$, that is the usual autocorrelation function, such as the one of Eq. (2b), but with N set to 1.

When dealing with experimental raw data, one never gets an ensemble average autocorrelation function, but only an average of the autocorrelation function $G'(t)$ over the time, T, of acquisition:

$$\begin{aligned}\langle G'(\tau)\rangle_T &= 1 + h(\tau)\left\langle \frac{1}{[\langle N(t)\rangle\langle N(t+\tau)\rangle]^{1/2}} \right\rangle_T \\ &= 1 + g(\tau)\end{aligned} \tag{6}$$

If the law of variation of the intensity is known (for instance an exponential series as given by Eq. 1), the time evolution of $I(t)$ [resp. $N(t)$] reads $I(t) = I_0 \times f(t)$ [resp. $N(t) = N_0 \times f(t)$], so that $g(\tau)$ can be rewritten:

$$g(\tau) = \frac{h(\tau)}{N_0}\left\langle \frac{1}{[\langle f(t)\rangle\langle f(t+\tau)\rangle]^{1/2}} \right\rangle_T \tag{7}$$

where N_0 is the number of molecules at the beginning of the acquisition and $f(t)$ is the decay function. In practice several evaluations of the term $\langle 1/[\langle f(t)\rangle\langle f(t+\tau)\rangle]^{1/2}\rangle_T$ indicated that it is almost independent of τ and only dependent on T and on the photobleaching rate. Therefore this term behaves like a constant A, so that the autocorrelation function of the fluorescence raw data corrected using the rectifying procedure reads:

$$\langle G'(\tau)\rangle_T = 1 + \frac{A}{N_0} g_{\mathrm{D}}(\tau) \tag{8}$$

Numerical Methods

Let us consider the diffusion equation in the presence of a first order irreversible chemical reaction induced by the laser field:

$$\frac{\partial C(\vec{r},t)}{\partial t} = D\Delta C(\vec{r},t) - \sigma_B \phi(\vec{r}) C(\vec{r},t) \tag{9a}$$

where $C(\vec{r},t)$ is the concentration of fluorescent molecules at point $\vec{r}$ and time t, D is the diffusion constant, σ_B is the photobleaching cross-section and $\phi(\vec{r})$ is the laser intensity

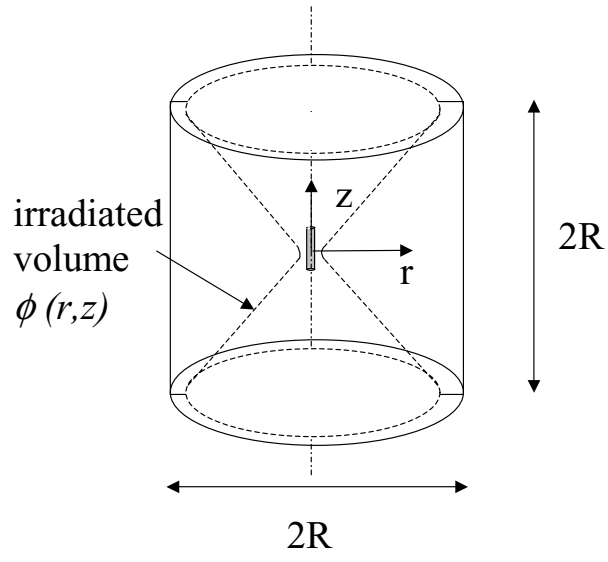

Fig. 1. Schematic view of the compartment used for the numerical resolution of Eq. (9). The grey cylinder corresponds to the confocal volume, where $C(r, z, t)$ is integrated to give the number of fluorescing molecules. The double cone symbolises the laser illumination profile $\phi(r, z)$.

at point $\vec{r}$ (in units of photon $\mathrm{s}^{-1}\cdot\mathrm{m}^{-2}$). Assuming that the laser intensity corresponds to the usual gaussian beam, $\phi(\vec{r})$ is given by:

$$\phi(\vec{r}) = \frac{2P}{\pi\omega(z)^2}\, e^{-2r^2/\omega(z)^2} \tag{9b}$$

$$\omega(z) = \omega_0[1 + (z/z_{\mathrm{R}})^2]^{1/2} \tag{9c}$$

where r represents the radial coordinate and z the coordinate along the axis (as depicted in Fig. 1), P is the laser power (in units of photon s^{-1}), ω_0 is the laser waist (0.25 μm) in the focal plane of the objective and z_{R} is the Rayleigh distance (0.5 μm).

To solve numerically Eq. (9a), it is interesting to consider the simple geometry of a cylindrical compartment, oriented and centred along the laser beam. For this particular geometry, the problem can be reduced to a 2D situation, taking advantage of the rotational invariance. Thus Eq. (9a) can be rewritten:

$$\begin{aligned}\frac{\partial C(r,z,t)}{\partial t} &= D\Delta_{r,z} C(r,z,t) + D\frac{1}{r}\frac{\partial C(r,z,t)}{\partial r} \\ &\quad -\sigma_B \phi(r,z) C(r,z,t)\end{aligned} \tag{10}$$

where the notation Δ_{rz} represents the Laplacian in cylindrical coordinates with rotational invariance $1/r(\partial^2/\partial r^2)r + \partial^2/\partial z^2$. The integration domain is then reduced to a rectangular section (a square in practice) of the cylinder containing the axis, as presented in Fig. 1, defined by $-R < r < R$ and $-R < z < R$.

The boundary conditions at the edge of the compartment are fixed by mass conservation: the mass flux has to cancel at the boundary, which implies that the gradient of C vanishes at the edges of the domain. Thanks to the symmetries of the problem (invariance through $r \to -r$ and $z \to -z$), the cancellation of the flux at the boundaries is equivalent to periodic boundary conditions on the square domain. The 2D diffusion Eq. (10) can then be solved in the Fourier space. If **k** corresponds to a wave-vector, Eq. (10) can be written in a discrete form as:

$$C_{\mathbf{k}}^{t+dt} = C_{\mathbf{k}}^{t} - k^2 D\, dt\, C_{\mathbf{k}}^{t+dt} + dt \left\{ D \frac{1}{r} \frac{\partial C(r,z,t)}{\partial r} - \sigma_B \phi(r,z) C(r,z,t) \right\}_{\mathbf{k}}^{t} \tag{11}$$

where index **k** stands for a Fourier transformation, k^2 is the square of the modulus of **k** and t is the time at which the quantity is evaluated. We can note on this equation that we evaluate the Laplacian in the right-hand term at time $t + dt$, which corresponds in fact to an implicit scheme ensuring a better convergence of the method. The solution can then be easily obtained from an initial guess of the concentration field $C(r, z)$ (in practice a homogeneous system), by iterating the relation:

$$C_{\mathbf{k}}^{t+dt} = \frac{1}{1 + k^2 D\, dt} \left[C_{\mathbf{k}}^{t} + dt \left\{ D \frac{1}{r} \frac{\partial C(r,z,t)}{\partial r} - \sigma_B \phi(r,z) C(r,z,t) \right\}_{\mathbf{k}}^{t} \right] \tag{12}$$

where the non-linear term between braces has to be estimated in the direct space at each time step and Fourier transformed to obtain the new estimate $C_{\mathbf{k}}^{t+dt}$ that has to be transformed back to obtain $C(r, z, t + dt)$. Due to the presence of the factor $1/r$, inducing an artificial singularity along the axis if care is not taken, we extrapolate the quantity $\frac{1}{r}\frac{\partial C(r,z,t)}{\partial r}$ to estimate its value at $r = 0$. We use in practice a square mesh to discretize the square domain, the number of points depending on the diameter of the vesicle: for a 20-μm vesicle, we use 200 $\times$200 grid points while a 60-μm vesicle requires 600 $\times$600 grid points to keep a comparable resolution. The time step can be varied from 10^{-3} times the diffusion time, to 10^{-6} (depending again on the requested precision). To compare with experiments, fluorescence can be estimated by an integration of $C(r, z, t + dt)$ in a small cylindrical region (the grey cylinder in Fig. 1), providing the number of fluorescent molecules in the confocal volume, N_{CV}. Please note that in practice, this cylinder is much smaller than the compartment itself, since the measurement cylinder has a diameter of 0.5 μm, for a height of 2.5 μm, while the compartment diameter goes from 20 to 60 μm.

RESULTS

Theoretical Approach

Hereafter we are interested in giving an approximate solution to the diffusion Eq. (9a). Following the theory of Sturm-Liouville equations [26], the general solution of Eq. (9a) can be expanded in a series of exponential decays:

$$C(\vec{r}, t) = \sum_i a_i c_i(\vec{r})\, e^{-k_i t} \tag{13}$$

where $-k_i$ and $c_i(\vec{r})$ are the eigenvalues and eigenfunctions of the time independent differential equation associated to the diffusion equation. The coefficients a_i are chosen in order to satisfy the initial condition at time $t = 0$ (laser switching on), that is a uniform concentration:

$$C(\vec{r}, 0) = C_0 = \sum_i a_i c_i(\vec{r}) \tag{14}$$

The short time behaviour of $C(\vec{r}, t)$ is given by the higher decay rate that enters in the expansion (13), which, in turn, is related to the initial decomposition (14). The derivation of the corresponding value is not straightforward. However, one can notice that for times significantly shorter than the mean dwell time τ_ω in the laser waist ω_r ($\tau_\omega \cong \omega_r^2/4D$), the diffusion does not play any significant role. Therefore, for $t \ll \tau_\omega$ the decay of $C(\vec{r}, t)$ is very fast close to the focus of the laser beam and negligible far from it. Since, for the experiments reported in this paper, $\tau_\omega \cong 30\ \mu$s, the short time bleaching regime cannot be observed by recording the fluorescence at a low frequency sampling rate. On the contrary, as shown in the Experimental Results section, FCS makes it possible to measure the bleaching rate in the confocal volume, since it gives access to very short time behaviours (down to about 1 μs).

We now focus on the regime attained at long times. In this so-called quasi-stationary regime, all the terms of expansion (13) vanish, except the slowest one, such that Eq. (13) can be rewritten:

$$C(\vec{r}, t) = c_1(\vec{r})\, e^{-k_1 t} \tag{15}$$

In order to derive an estimate of the quasi-stationary bleaching rate k_1, we consider the time evolution of the total number of molecules, $N(t)$, contained within the vesicle:

$$N(t) = \int_{\mathrm{Ves}} C(\vec{r}, t)\, d\vec{r} \tag{16}$$

then:

$$\frac{dN}{dt} = \int_{\text{Ves}} \frac{\partial C}{\partial t}\, d\vec{r} \tag{17}$$

Inserting Eq. (9) into Eq. (17) yields:

$$\frac{dN}{dt} = \int_{\text{Ves}} [D\Delta C(\vec{r}, t) - \sigma_B \phi(\vec{r}) C(\vec{r}, t)]\, d\vec{r} \tag{18}$$

Because the term $D\Delta C(\vec{r}, t)$ vanishes after integration due to the boundary condition at the compartment surface, inserting Eq. (15) into Eq. (18) reduces it to:

$$\frac{dN}{dt} = -\sigma_B\, e^{-k_1 t} \int_{\text{Ves}} \phi(\vec{r}) c_1(\vec{r})\, d\vec{r} \tag{19}$$

On the other hand, inserting Eq. (15) into Eq. (17) leads to:

$$\frac{dN}{dt} = -k_1\, e^{-k_1 t} \int_{\text{Ves}} c_1(\vec{r})\, d\vec{r} \tag{20}$$

From Eqs. (19) and (20) we conclude that:

$$k_1 = \sigma_B \tilde{\phi} \tag{21}$$

with:

$$\tilde{\phi} = \frac{\int_{\text{Ves}} \phi(\vec{r}) c_1(\vec{r})\, d\vec{r}}{\int_{\text{Ves}} c_1(\vec{r})\, d\vec{r}} \tag{22}$$

However, in the case of weak photobleaching, the concentration depletion is weak, such that $c_1(\vec{r})$ is almost constant. Consequently:

$$\tilde{\phi} \cong \frac{\int_{\text{Ves}} \phi(\vec{r})\, d\vec{r}}{\int_{\text{Ves}} d\vec{r}} = \bar{\phi} \tag{23}$$

Assuming a top hat profile for the laser beam, with an aperture half angle of 33° (corresponding to the 1.2 N.A. of the water objective), one obtains $\phi = 0.41 \times P/R^2$, where P is the laser power (in photon/s) and R is the vesicle radius. From Eqs. (21) and (23) one immediately deduces, in the case of weak photobleaching, that:

$$k_1 \cong 0.4\, \sigma_B \frac{P}{R^2} \tag{24}$$

This approximation is valid as long as the concentration depletion in the laser beam is weak. It implies that the probability for a molecule to be photobleached, when it diffuses through the laser beam, must be much smaller than 1. Let us consider a plane, perpendicular to the laser axis, where the laser beam radius is ρ and the intensity is $P/\pi\rho^2$. According to the laws of diffusion, the average time taken by a molecule to cross the laser beam of diameter 2ρ is about $(2\rho)^2/4D = \rho^2/D$. Then the condition of weak photobleaching reads:

$$\sigma_B \frac{P}{\pi\rho^2} \times \frac{\rho^2}{D} \ll 1 \tag{25a}$$

or, by introducing the photobleaching parameter $p_B = \sigma_B P/D$:

$$p_B \ll 1 \tag{25b}$$

In this regime, the molecules explore the whole compartment before being photobleached and therefore the relevant laser intensity is averaged over the accessible volume, as given by Eq. (23). It is worth to note that in the case of weak photobleaching (i.e. fast diffusion) the photobleaching decay time, $\tau_1 = 1/k_1 \cong 2.5\frac{R^2}{\sigma_B P}$, is much larger than the diffusion time through the vesicle, $T_R \cong R^2/6D$. Correspondingly, the time necessary for the quasi-stationary regime to be established is given by τ_R.

Numerical Results

As described above, the quasi-stationary regime is established when the diffusion through the whole compartment has taken place. During the time of diffusion, τ_R, the shape of the concentration hole varies, as one can see in Fig. 2 by comparing 3D plots of the

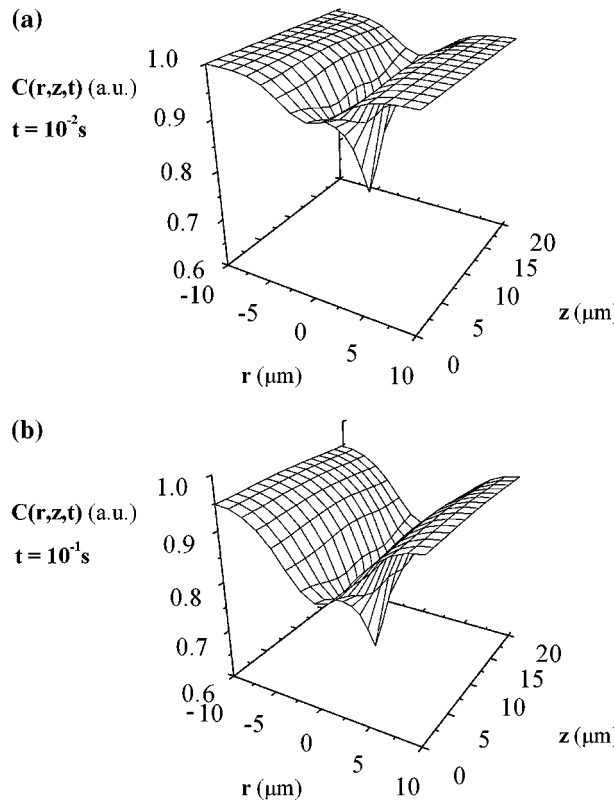

Fig. 2. 3D representation of the calculated concentration of fluorescent molecules within the compartment, $C(r, z, t)$, at two different times: (a) $t = 0.01$ s; (b) $t = 0.1$ s. The diffusion time, τ_R, through the compartment ($R = 10\ \mu$m) is about 0.05 s ($D = 3\times 10^{-6}$ cm^2/s). Note that this time lies between $t = 0.01$ s (a) and $t = 0.1$ s (b).

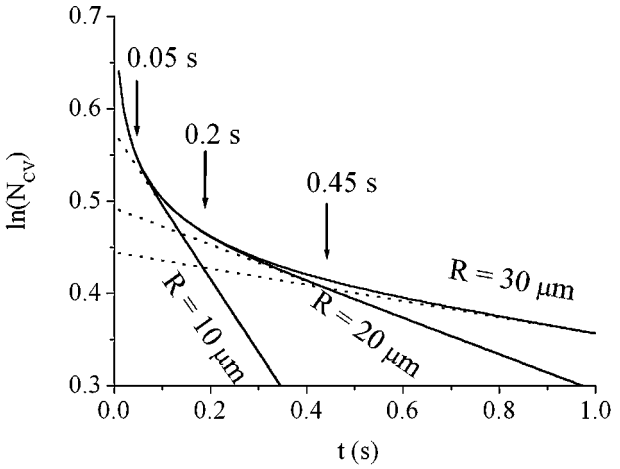

Fig. 3. Calculated fluorescence decays for various compartment sizes (see Materials and Methods section). The radii of the compartments are indicated close to the corresponding curves. The dotted lines are the long time fits. The times of diffusion through the compartment radii, $\tau_R = R^2/6D$, are indicated by the arrows. The diffusion regime corresponds to the parameter $p_B = 0.1$, i.e. to a weak photobleaching (see Eq. 25).

concentration, calculated with a vesicle of radius $R = 10\ \mu$m and $D = 3 \times 10^{-4}$ cm^2/s, at two different times. The time of diffusion through the vesicle radius, τ_R, is about 0.05 s, which lies between $t = 0.01$ s (Fig. 2a) and $t = 0.1$ s (Fig. 2b). Interesting enough is that the time evolution of the concentration can be conveniently put into evidence by monitoring the number of fluorescent molecules in the confocal volume, $N_{CV}(t)$. As can be seen in Fig. 3, the very short time behaviour is clearly independent of the compartment size for three different vesicles of radii 10, 20 and 30 μm. This agrees with the discussion in the previous section. Conversely, for the long time behaviour (i.e. $t > \tau_R$) one sees that the larger the vesicle diameter, the slower the concentration decrease, in agreement with Eq. (24). In addition, the exponential regime is clearly reached after the characteristic time τ_R.

An important (and somewhat unexpected) result of the present theoretical and numerical study is that the photobleaching rate k_1 is independent of the diffusion constant D, provided that the fast diffusion condition is fulfilled, i.e. when $D \gg \sigma_B P$ or $p_B \ll 1$. Conversely, in the slow diffusion regime, k_1 becomes dependent on the diffusion coefficient, because any molecule entering the laser beam is photobleached ($p_B \geq 1$). Consequently the photobleaching decay rate is driven by the diffusion of molecules through the compartment, towards the laser beam. One can see in Fig. 4 the influence of the parameter p_B on the photobleaching rate.

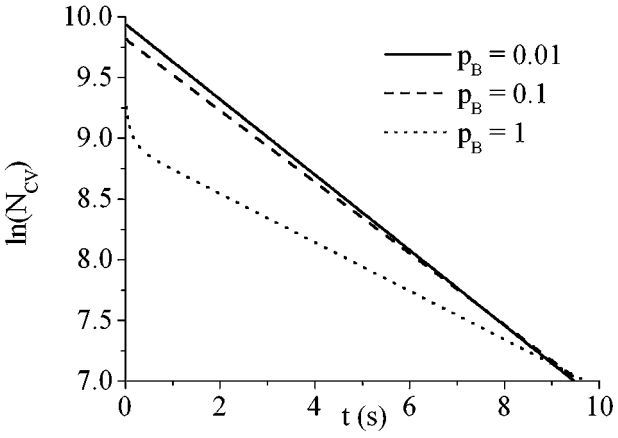

Fig. 4. Calculated fluorescence decays for various values of the photobleaching parameter p_B in a vesicle of radius $R = 10\ \mu$m. As long as $p_B \ll 1$ the photobleaching rate marginally depends on p_B, in contrast to the case $p_B \geq 1$. The curve with $p_B = 0.1$ is also shown in Fig. 3 where the time scale is limited to $t < 1$ s.

Experimental Results

Photobleaching in Solution

Experiments were performed with two fluorochromes having very different propensities to photobleach. While LY-CH appears to be stable in solution with the laser powers used, one observes in Fig. 5 a decrease of the fluorescence rate of FITC at laser powers above about 10 μW. Since this photobleaching behaviour is not

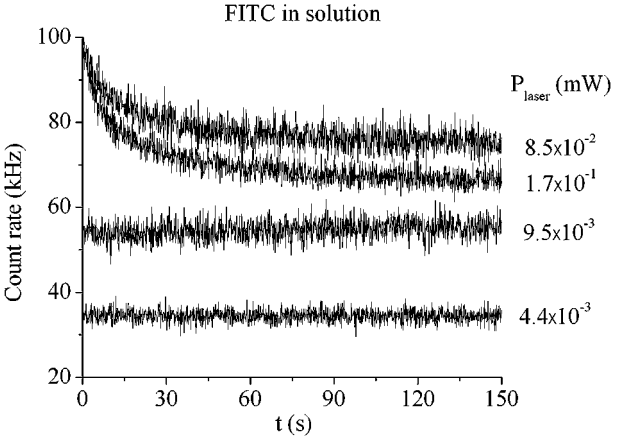

Fig. 5. Examples of the fluorescence count rate behaviour of FITC in solution (20 nM), measured for various laser powers. The fluorescence intensity shows a significant decay for laser powers above about 10^{-2} mW, which means that the photobleaching of molecules is no more balanced by the flow of incoming intact molecules. Due to this photobleaching effect, the fluorescence count rate corresponding to the higher laser power (1.7×10^{-1} mW) quickly reaches a value lower than that corresponding to 8.5×10^{-2} mW.

concerned by compartmentalisation, we will not describe its kinetic [27].

Complementary experiments (data not shown) have been performed by illuminating uniformly, with a high power laser (Coherent Innova 200), wells (1 mm deep and a few mm wide) containing solutions of fluorochromes. The corresponding fluorescence decay rates are therefore independent of the diffusion which allows to directly measure the photobleaching cross sections: $\sigma_B \cong 2.5 \times 10^{-21}$ cm^2 for LYCH at $\lambda = 457$ nm and $\sigma_B \cong 4 \times 10^{-20}$ cm^2 for FITC at $\lambda = 488$ nm. We note that this value for the photobleaching cross sections of FITC is larger than the value implicitly given by Widengren [8] (about 10^{-20} cm^2).

Photobleaching in Vesicles

The most important consequence of compartmentalisation is that, for laser powers where the corresponding fluorescence rate in solution is constant (which is always the case in the reported experiments, unless specified), photobleaching becomes observable, as shown in Figs. 6 and 7 for FITC and LY-CH. These figures clearly show the expected influence of the vesicle size and of the laser power on the photobleaching time. Note that the decay times τ_1 indicated in the figures are the shortest times of the multi-exponential fits (see Eq. 9). Up to now, we have not studied in detail the origin of the longer decay times and we assume τ_1 to correspond to the decay time of the theoretical analysis. In order to quantitatively assert the theoretical analysis, let us rewrite Eq. (24) by introducing

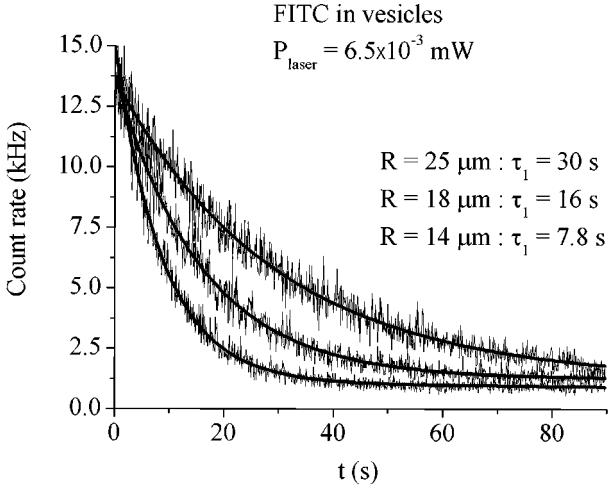

Fig. 6. Variation of the fluorescence decays of FITC with the vesicle radius. All the vesicles come from the same preparation, with a FITC concentration of 20 nM. The laser power is set to a value such that the fluorescence count rate would be constant in solution (see Fig. 5).

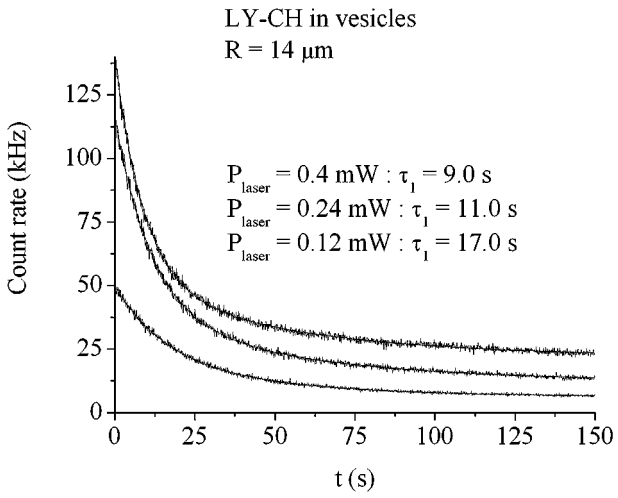

Fig. 7. Variation of the fluorescence decays of LY-CH with the laser power. All the vesicles have about the same radius and come from the same preparation, with a LY-CH concentration of 20 nM. The laser power are set to values such that the fluorescence count rate would be constant in solution.

a photobleaching dose, U_1, defined by:

$$U_1 = \tau_1 \times P = 2.5 \frac{R^2}{\sigma_B} \tag{26}$$

P being expressed in photons/s, this equation can be interpreted as the number of photons that must cross the vesicle to deplete the fluorescence rate by a factor e. Figure 8 clearly shows that the experimental results are in good agreement with Eq. (26). It must be noticed that an important source of uncertainty comes from the vesicle diameter measurements. By fitting the experimental data one can estimate the photobleaching cross section,

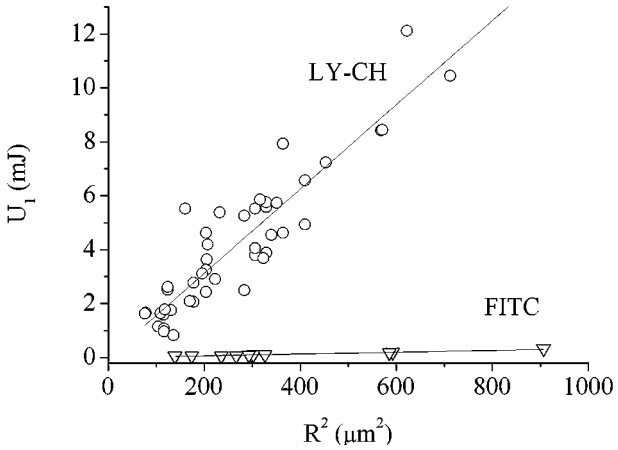

Fig. 8. Photobleaching dose, U_1, versus the square of the vesicle radius. This plot is obtained by compiling data obtained with various laser powers. The photobleaching propensity of FITC is about 50 times larger than that of LY-CH.

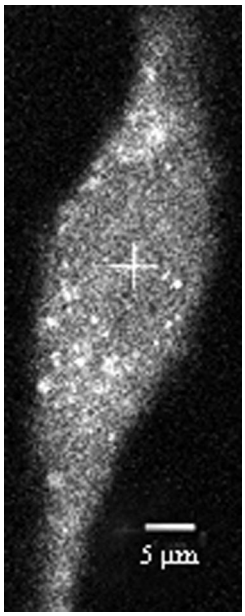

Fig. 9. Image of a living cell acquired using the confocal laser scanning microscope. Due to the low fluorescent level required for FCS, pinhole was slightly open. FCS was performed in the nucleus, at the point indicated by the cross.

$\sigma_B = 7.0 \times 10^{-22}$ cm^2 for LY-CH and $\sigma_B = 3.1 \times 10^{-20}$ cm^2 for FITC. In the case of FITC this value agrees well with the results obtained by illuminating uniformly the solution while there is a discrepancy of a factor 3 for LYCH (see above).

Photobleaching in Living Cells

FCS was performed on ten living cells at two laser powers (Fig. 9). FITC photobleaching, as observed on the count rate curves, was significant even at the lowest laser power and increased with the laser power (Fig. 10). As expected, photobleaching is more pronounced than in solution (see Fig. 5), due to compartmentalisation. The cell itself represents a compartment like a vesicle, but it includes many domains and sub-domains.

Fluorescence Correlation Spectroscopy in Solution

When the laser power is low enough, such that the fluorescence rate is stationary in solution, the molecules have nevertheless a non zero probability to be photobleached during their dwell time within the confocal volume. To put into evidence the photobleaching probability by using the autocorrelation function, we performed experiments in solution, at various laser powers, on LY-CH and FITC (Figs. 11 and 12). One immediately observes, in both figures, that the amplitude of the autocorrelation function

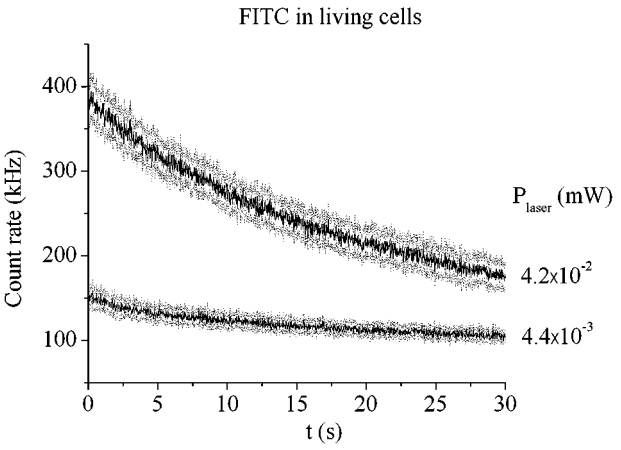

Fig. 10. Variation of the fluorescence decays of FITC in living cells. Measurements were performed in ten cells at positions located in the nucleus and at two laser powers. Mean ± s.e.m. curves were figured out.

decreases with the laser power. This may be due to the saturation of the transition: as the laser power increases, the fluorescence rate saturates, while the elastic and inelastic Raman scattering rates linearly increase. As already discussed in the literature [28], this results in a decrease of the autocorrelation amplitude. This effect will be taken into account in the following, when deriving the number of fluorescent molecules from the autocorrelation amplitude

The autocorrelation curves of LY-CH were fitted using Eq. (3), while fixing the diffusion time at $\tau_D = 19$ μs. The fitted value of k_B increases linearly with the laser power as shown in the inset of Fig. 11 (the triplet

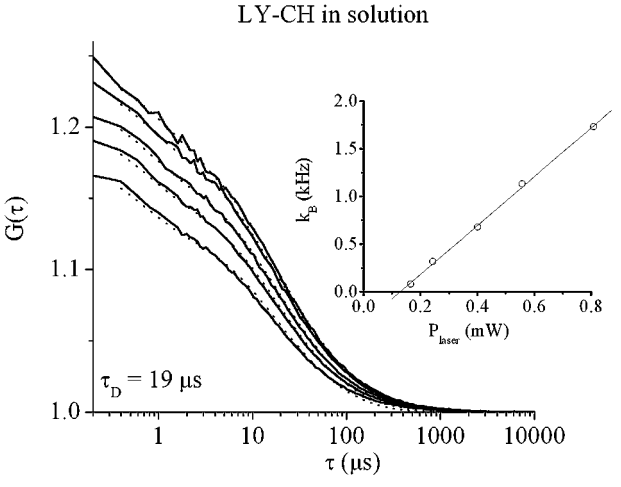

Fig. 11. Autocorrelation curves of LY-CH in solution, at increasing laser powers: 0.16 mW, 0.24 mW, 0.40 mW, 0.56 mW and 0.81 mW, from top to bottom curves (at these laser powers the fluorescence count rate is constant in solution). By fixing the diffusion time τ_D to a constant value of 19 μs, one observes in the inset that the photobleaching rate, k_B, within the confocal volume increases with the laser power.

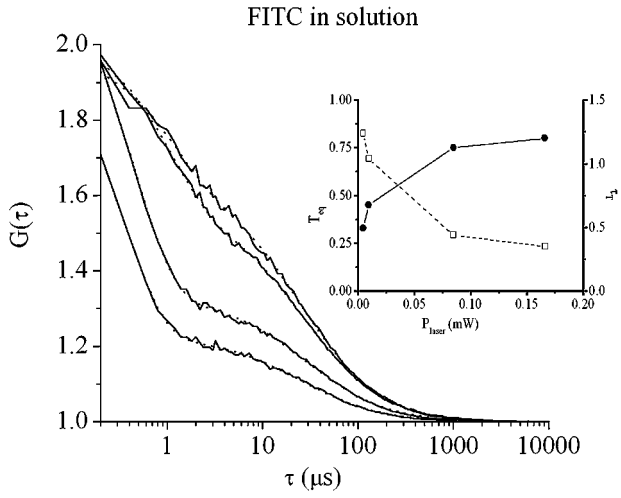

Fig. 12. Autocorrelation curves (solid lines) of FITC in solution, at increasing laser powers: 4.4×10^{-3}, 9.5×10^{-3}, 8.5×10^{-2} and 1.7×10^{-1} mW, from top to bottom curves. The dotted lines correspond to the fits. One observes in the inset that the triplet fraction, T_{eq} increases with the laser power (solid circles), while the triplet time, τ_T, decreases (open squares).

parameters, T_{eq} and τ_T being almost constant. This value of 19 μs corresponds to a fit performed at a laser power of 0.083 mW. Note that, for the laser powers used, the photobleaching probability, is very low ($k_B \times \tau_D \ll 1$), which corresponds to the fast diffusion regime (Eq. 25). Despite the fact that the fits of the autocorrelation functions are not very good, we took benefit from the linear relationship between k_B and the laser power to estimate the photobleaching cross section of LY-CH:

$$k_B \cong \sigma_B \frac{P}{\pi \omega_r^2} \tag{27}$$

where P is the laser power expressed in photon/s. From the measured value of τ_D (19 μs) and using the same value of D (2.8×10^{-6} cm^2/s) than for Rh6G (because of the similar molecular weights of Rh6G and LY-CH), we calculated $\omega_r = \sqrt{4D\tau_D} = 0.15$ μm. The slope of the linear relationship between k_B and P_{laser} being 2.6 kHz/mW, we deduce $\sigma_B = 7.8 \times 10^{-22}$ cm^2. Taking into account the poor quality of the autocorrelation fits, this value of σ_B is surprisingly close to the one obtained from the photobleaching rate in compartment, that is 7.0×10^{-22} cm^2.

The autocorrelation curves obtained with FITC (Fig. 12) behave differently than for LY-CH and are nevertheless very similar to the results reported by Widengren [29]. Since the corresponding experiments have been performed at laser powers where the fluorescence intensity is significantly affected by photobleaching effects (see Fig. 5), we calculated the autocorrelation curves at times longer than 90 s, where the fluorescence intensity reaches a stationary regime. As shown in the inset, strong effects are observed on the triplet fraction, T_{eq}, (which increases with the laser power) and on the triplet time, τ_T, (which decreases with the laser power). Conversely, the photobleaching of FITC could not be put into evidence with parameter k_B, despite the very high photobleaching cross section of FITC measured in vesicles ($\sigma_B = 3.1 \times 10^{-20}$ cm^2). We suggest that this may be due to the saturation of the transition and to the triplet population in the centre of the confocal volume. The consequence of these phenomena is an apparent increase of the confocal volume radius ω_r, that counterbalances the photobleaching effect when the laser power is increased [29]. Note that for LY-CH, the triplet population and the saturation are lower, as indicated by the variation of the autocorrelation curves, (compare Figs. 11 and 12) so that photobleaching can be put into evidence by analysing the autocorrelation function.

Fluorescence Correlation Spectroscopy in Vesicles

As shown in Fig. 13a, the autocorrelation function calculated over a period of time where the fluorescence intensity strongly decreases is significantly biased and, clearly, cannot be fitted with a standard diffusion model. We have therefore investigated two different strategies in order to recover a unbiased autocorrelation function: the rectifying and the time slicing methods (see the Materials and Methods section).

Figure 13a shows that the so called rectifying procedure significantly modifies the shape of the autocorrelation function in the case of strong fluorescence decay due to photobleaching. Conversely, when the intensity variation over the range used to calculate the autocorrelation is less than typically 10%, the correction is insignificant. The time slicing method appeared to give identical results to those of the rectifying method, as one can see in Fig. 13b. A procedure analogous to our time slicing method has been proposed by Chen *et al.* [30] when performing Photon Counting Histogram on eGFP in vivo.

In order to numerically evaluate the validity of the above mentioned corrections, we calculated the average number of molecules in the confocal volume, $\langle N(t) \rangle$, for a series of 5 successive, 30 s long, time ranges. This implies several steps: first, applying the rectifying or time slicing procedure to each time range; then adjusting the amplitude of autocorrelation curves. Note that in the case of a strong fluorescence decay the amplitude adjustment must be done twice: the first adjustment corresponds to formula (8) and is based on the shape, $f(t)$, of the intensity decay; the second adjustment corrects the autocorrelation amplitude from the consequences of the relative increase of the

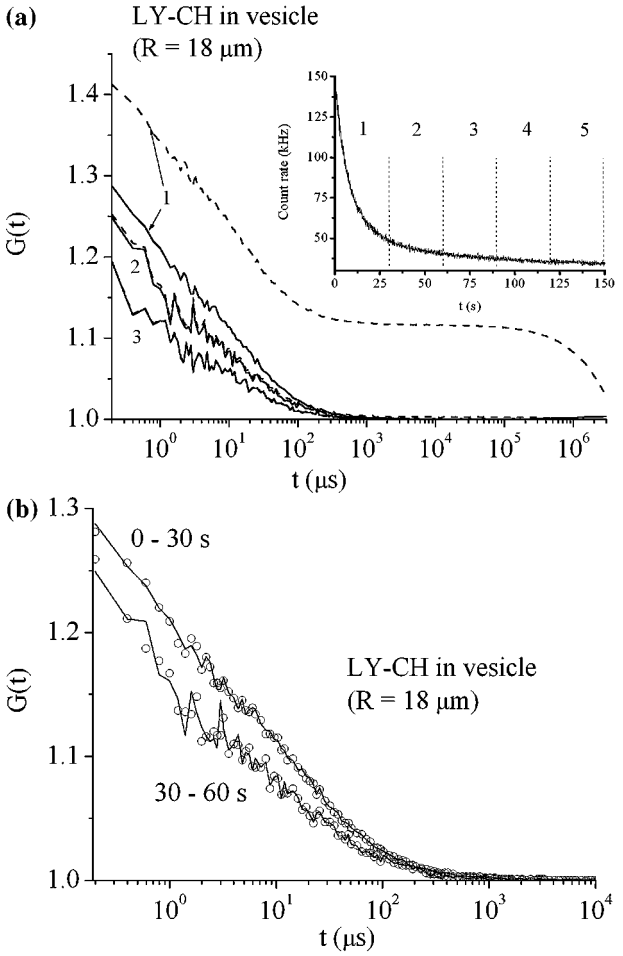

Fig. 13. Autocorrelation curves of LY-CH in a vesicle of radius $R = 18\ \mu$m at a laser power of 0.81 mW. Dotted lines correspond to original raw data, solid lines (resp. circles) correspond to raw data corrected with the rectifying (resp. time slicing) method. (a): effect of the fluorescence decay for the three first time slices of the fluorescence trace (see inset); the autocorrelation curves of the first time slice ($n^\circ 1$) is significantly biased by the fluorescence decay, such that the corresponding correction is important. Conversely the autocorrelation curve of the second time slice ($n^\circ 2$) is marginally affected by the photobleaching, while from the third time slice original and corrected raw data give superimposed autocorrelation curves ($n^\circ 4$ and 5 not shown). (b): comparison between the two raw data correction methods applied to the two first time slices (30 s long); the agreement between the two methods is very satisfying, even in the case of strong photobleaching.

elastic and inelastic scattered light in the total count rate I. This correction is done by assuming that the amount of scattered light, I_s, is given by the residual count rate at long time, i.e. by the constant A_0 in the count rate decay fit (see Eq. 9). By multiplying the autocorrelation amplitude by the constant $I^2/(I - I_s)^2$ [28], one sees in Fig. 14 that the agreement between the count rate (corrected from the

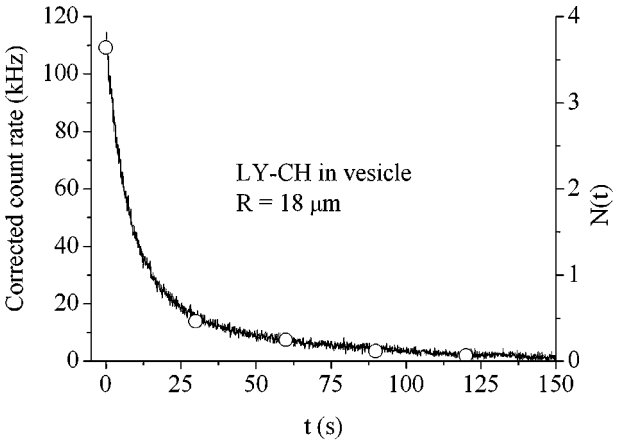

Fig. 14. Simultaneous plots of the fluorescence count rate decay, corrected from the base line contribution (left axis) and of the number of molecules calculated from the corrected autocorrelation curves (see text).

scattered light contribution) and the number of molecules determined by the corrected autocorrelation curve is very satisfactory. In contrast, a simplistic analysis of Fig. 13b based on the relation $\langle N \rangle = [G(0) - 1]^{-1}$ would suggest that there are more molecules between 30 and 60 s than between 0 and 30 s!

Fluorescence Correlation Spectroscopy in Living Cells

As already mentioned, from the point of view of photobleaching living cells are expected to behave like compartments, thus the decay of the fluorescence due to photobleaching is expected to affect the autocorrelation curve shape. Figure 15 shows the autocorrelation functions corresponding to the first and the last, 5 s long, time ranges of Fig. 10. Unbiased autocorrelation functions were calculated using both the rectifying and the time slicing methods, like in vesicles. The correction was more significant for the first time slice where the fluorescence decay is more pronounced (compare in Fig. 14, the first and last 5 s time slices). Autocorrelation curves were fitted, and reliable adjustments were obtained using either the anomalous or the free 3D two-component diffusion model. Note that after correction for photobleaching, estimated second diffusion times and anomalous coefficients were significantly modified [6]. In this particular case, unlike the previous section, the relative fluorescence decay is weak. This allows to estimate immediately the number of fluorescent molecules in the confocal volume using the simple formula $\langle N \rangle = [G(0) - 1]^{-1}$ where $G(t)$ is the corrected autocorrelation functiun. We see that in this case $\langle N \rangle$ decreases by a factor of 2 after illumination for 30 s at a laser power of 4.2×10^{-2} mW.

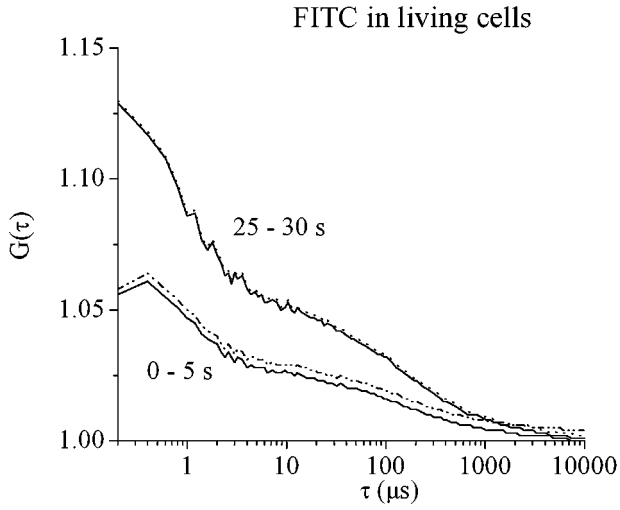

Fig. 15. Autocorrelation curves of FITC in living cells, at the highest laser power (0.042 mW), for the first acquisition (0-5 s, botton curves) and the last one (25–30 s, top curves). Dotted lines: original raw data, solid line: data corrected with the time slicing method. Measurements were performed in ten cells and the mean curves are shown. Photobleaching is more significant during the first 5 s (see Fig. 10) and the correction is thus more significant. In this case the quantity $1/[G(0)-1]$ provides a good estimation of the number of molecules in the confocal volume. As expected this number is lower after 25 s of irradiation.

DISCUSSION AND CONCLUSION

When photobleaching takes place in a compartment (that of a vesicle or a cell), two rates must be compared: the first one is the photobleaching rate that would occur if the laser power were distributed uniformly over the whole compartment; the second is the diffusion rate through that compartment. The photobleaching rate observed at long times is determined by the slowest of those two characteristic rates. As a matter of fact, if the diffusion is fast enough (i.e. the molecules are small enough, $D \gg \sigma_B P$), the photobleaching rate does not depend on the diffusion constant and is determined by the laser intensity averaged over the compartment, that is $k_1 \propto \sigma_B P/R^2$. Conversely, if the diffusion is slow (i.e. the molecules are large, or involved in a large molecular complex or transiently immobilised due to an interaction), the input of unbleached molecules into the irradiated region determines the photobleaching rate, that scales as D/R^2. Note that in both cases, the photobleaching rate observed at long time is dependent on the size of the compartment or sub-domain. This explains why the photobleaching rate in living cells is larger compared with the situation in solution and, partly, why the photobleaching is heterogeneous inside cells [31]. Note that the photobleaching rate at very short time is independent on both the diffusion and compartment size and only dependent on the photostability of the fluorochrome and the laser power.

When performing FCS, one usually wants to measure the concentrations of the various molecular components that are simultaneously present in the confocal volume. If all the components satisfy the fast diffusion condition, $D \gg \sigma_B P$, they all photobleach at the same rate ($k_1 \propto \sigma_B P/R^2$) and their relative concentrations are constant along the decay time. Consequently, one can average the autocorrelation curves of the consecutive time slices to obtain concentrations and diffusion constants. Conversely, when some of the components are in the fast diffusion regime and some other are not, the photobleaching rate varies from $\sigma_B P/R^2$ for the fastest component down to D/R^2 for the slowest one, so that the relative concentrations change during the fluorescence decay. In that case, it is not valid to average the autocorrelation curves of the consecutive time slices. However, these autocorrelation curves must give an evolution of the concentrations that is consistent with the photobleaching rates which can be deduced from the laser power, the photobleaching cross section, the compartment size and the diffusion constants.

At this point it is interesting to evaluate the highest molecular weight (MW) of a FITC labelled molecule such that one is still in the fast diffusion regime. According to Eq. (25), this condition reads $D \gg \sigma_B P$. Assuming a laser power of about 10^{-2} mW, e.g. $\cong 10^{13}$ photons/s (corresponding to a count rate of several tens of kHz per molecule), a photobleaching cross section $\sigma_B \cong 10^{-20}$ cm^{-2}, the fast diffusion condition is satisfied for $D \gg 10^{-7}$ cm^2/s, that is for MW $\ll 20 \times 10^6$ g/mol. Note that this upper limit of the MW corresponds to a globular molecule in aqueous solution. In living cells, where the viscosity is typically 3 to 5 times larger, the fast diffusion condition rather corresponds to MW $\ll 10^6$ g/mol. This limit would be significantly higher for more stable fluorophores with fluorescence quantum yield high enough for acquisition at low laser power, such as Alexa (Molecular Probes), Cynanine (Amersham) and also the natural fluorescent protein eGFP ("enhanced Green Fluorescent Protein"). For such dyes the slow diffusion regime would only concern transiently immobilised molecules, following interaction, making data interpretation straightforward.

Last but not least, it is worth to note that, knowing the fluorescence decay rate, k_1, and the photobleaching constant within the confocal volume, k_B, one can combine Eqs. (24) and (27) to evaluate the size R of the compartment: $k_B/k_1 \cong (R/\omega_r)^2$. Of course this evaluation is feasible, providing one is able to properly analyse the autocorrelation curve to a get reliable value of k_B. Unfortunately, when several components are simultaneously

presents (which is the interesting case) this goal is probably difficult to reach.

ACKNOWLEDGMENTS

This work was supported the "Action Concertée Incitative, Physico chimie de la matière complexe." The authors thank B. Batteux for valuable technical help and Professor M. Robert Nicoud (IAB, Inserm U309) for his support in FCS development. We thank also Dr Annie Viallat for providing us material and methods for the formation of vesicles and numerous discussions.

REFERENCES

1. W. W. Webb (2001). Fluorescence correlation spectroscopy: Inception, biophysical experimentation and prospectus. *Appl. Opt.* **40**, 3969–3983.
2. D. Madge, E. Elson, and W. W. Webb (1972). Thermodynamic fluctuations in a reacting system-measurement by fluorescence correlation spectroscopy. *Phys. Rev. Lett.* **29**, 705–708.
3. E. L. Elson (2001). Fluorescence correlation spectroscopy measures molecular transport in cells. *Traffic* **2**, 789–796.
4. E. Haustein and P. Schwille (2003). Ultrasensitive investigations of biological systems by fluorescence correlation spectroscopy. *Methods* **29**, 153–166.
5. S. T. Hess, S. Huang, A. A. Heikal, and W. W. Webb (2002). Biological and chemical applications of fluorescence correlation spectroscopy: A review *Biochemistry* **41**, 697–705.
6. P. Schwille, U. Haupts, S. Maiti, and W. W. Webb (1999). Molecular dynamics in living cells observed by fluorescence correlation spectroscopy with one- and two-photon excitation.*Biophys. J.* **77**, 2251–2265.
7. P. S. Dittrich and P. Schwille (2001). Photobleaching and stabilization of fluorophores used for single molecule analysis with one- and two-photon excitation. *Appl. Phys. B* **73**, 829–837.
8. J. Widengren and R. Rigler (1996). Mechanisms of photobleaching investigated by fluorescence correlation spectroscopy. *Bioimaging* **4**, 149–157.
9. G. H. Patterson and D. W. Piston (2000). Photobleaching in two-photon excitation microscopy *Biophys J.* **78**, 2159–2162.
10. T. S. Chen, S. Q. Zeng, Q. M. Luo, Z. H. Zhang, and W. Zhou (2002). High-order photobleaching of green fluorescent protein inside live cells in two-photon excitation microscopy. *Biochem. Biophys. Res. Commun.* **291**, 1272–1275.
11. K. Bacia and P. Schwille (2003). A dynamic view of cellular processes by in vivo fluorescence auto- and cross-correlation spectroscopy. *Methods* **29**, 74–85.
12. K. Bacia, I. V. Majoul, and P. Schwille (2002). Title probing the endocytic pathway in live cells using dual-color fluorescence cross-correlation analysis. *Biophys. J.* **83**, 1184–1193.
13. L. Song, E. J. Hennink, I . T. Young, and H. J. Tanke (1995). Photobleaching kinetics of fluorescein in quantitative fluorescence microscopy. *Biophys. J.* **68**, 2588–2600.
14. L. Song, C. A. G. O. Varma, J. W. Verhoeven, and H. J. Tanke (1996). Influence of the triplet excited state on the photobleaching kinetics of fluorescein in microscopy. *Biophys. J.* **70**, 2959–2968.
15. L. Song, R. P. van Gijlswijk, I. T. Young, and H. J. Tanke (1997). Influence of fluorochrome labeling density on the photobleaching kinetics of fluorescein in microscopy. *Cytometry* **27**, 213–223.
16. C. Eggeling, L. Brand, and C. A. M. Seidel (1997). Laser-induced fluorescence of coumarin derivatives in aqueous solutions: Photochemical aspects for single molecule detection. *Bioimaging* **5**, 105–115.
17. C. Eggeling, J. Widengren, R. Rigler, and C. A. M. Seidel (1998). Photobleaching of fluorescence dyes under conditions used for single-molecule detection: Evidence of two-step photolysis. *Anal. Chem.* **70**, 2651–2659.
18. C. Eggeling, J. Widengren, R. Rigler, and C. A. M. Seidel (1999). In W. Rettig (Ed.), *Applied Fluorescence in Chemistry, Biology and Medicine*, Springer-Verlag, Berlin, pp. 193–240.
19. R. Peters, A. Brüngers, and K. Schulten (1981). Continuous fluorescence microphotolysis: A sensitive method for study of diffusion processes in single cells *Proc. Nat. Acad. Sci. U.S.A.* **78**, 962–966.
20. U. Kubitscheck, P. Wedekind, and R. Peters (1998). Three-dimensional diffusion measurements by scanning microphotolysis. *J. Microsc. (USA)* **192**, 126–138.
21. M. Wachsmuth, T. Weidemann, G. Müller, U. W. Hoffmann-Rohrer, T. A. Knoch, W. Waldekc, and J. Langowski (2003). Analyzing intracellular binding and diffusion with continuous fluorescence photobleaching. *Biophys. J.* **84**, 3353–3363.
22. G. Carrero, D. McDonald, E Crawford, G. de Vries, and M. J. Hendzel (2003). Using FRAP and mathematical modeling to determine the in vivo kinetics of nuclear proteins. *Methods* **29**, 14–28.
23. J. Lippincott-Schwartz, N. Altan-Bonnet, and G. H. Patterson (2003). Photobleaching and photoactivation: Following protein dynamics in living cells. *Suppl. Nat. Cell Biol.* **5**, S7–S14.
24. M. I. Angelova, S. Soléau, P. Méléard, J. Faucon, and P. Bothorel (1992). Preparation of giant vesicles by external A. C. electric field *Progr. Coll. Pol. Sci.* **89**, 127.
25. J. Enderlein (1996). Path integral approach to fluorescence correlation experiments. *Phys. Lett. A* **221**, 427–433.
26. R. Courant and D. Hilbert (1989). *Methods in Mathematical Physics*, Wiley, New York, Vol. I, ch. V.
27. J. Mertz (1998). Molecular photodynamics involved in multi-photon excitation fluorescence microscopy. *Eur. Phys. J. D* **3**, 53–66.
28. N. L. Thompson (1991). In J. R. Lakowicz (Ed.), *Topics in Fluorescence Spectroscopy*, Plenum Press, New York, pp. 337–378.
29. J. Widengren, U. Mets, and R. Rigler (1995). Fluorescence correlation spectroscopy of triplet states in solution: A theoretical and experimental study. *J. Phys. Chem.* **99**, 13368–13379.
30. Y. Chen, J. D. Müller, Q. Ruan, and E. Gratton (2002). Molecular brightness characterisation of EGFP in vivo by fluorescence fluctuation spectroscopy *Biophys. J.* **82**, 133–144.
31. D. M. Benson, J. Bryan, A. L. Plant, A. M. Gotto Jr., and L. C. Smith (1985). Digital imaging fluorescence microscopy: Spatial heterogeneity of photobleaching rate constants in individual cells. *J. Cell Biol.* **100**, 1309–1323